Ultrasonic properties of Mg23Al3Y4 alloy with LPSO structures

WILEY-VCH

DOI: 10.1002/ ((please add manuscript number))
Article type: Full Paper

Title Ultrasonic properties of $Mg_{23}Al_3Y_4$ alloy with LPSO structures

Mikio Fukuhara[*,1], *Mitsuhiro Takeda*[2], *and Kazuya Konno*[2]

[1] New Industry Creation Hatchery Center, Tohoku University, Sendai 980-8579, Japan
[2] Department of General Engineering, National Institute of Technology, Sendai College, Natori 981-1239, Japan

Corresponding author: E-mail: fukuhara@niche.tohoku.ac.jp

Keywords: $Mg_{23}Al_3Y_4$ alloy, LPSO structures, ultrasonic properties, *VEC*

Ultrasonic properties of $Mg_{23}Al_3Y_4$ alloy, which has a synchronized long-period stacking ordered (LPSO) structure, were examined in terms of valence electron concentration (*VEC*), and real and complex elasticities. The alloy locates to a point (2.54, 436.5 K) near a critical amorphous alloy composition, and a point with largest Poisson's ratio (0.322) and lower *G/K*(0.404) in metal group, showing a metastable like metallic alloy. The addition of small amounts of Al and Y elements, *i.e.* appearance of excess electrons induces an increase in c/a ratio and cell expansion of hcp Mg lattice, and stabilization of cluster structures, leading to formation of LPSO phases with $L1_2$ typed Al_6Y_8 clusters. The elasticity and viscoelasticity of the alloy is predominated by three-dimensional volumetric motion, *i.e.*, high rigidity.

1. Introduction Mg-based ordered alloys can be regarded as the last frontier of light-metals and metallic alloys. Much attention has been devoted to enhancement of strengthening by synchronized long-period stacking ordered (LPSO) structure in Mg-based alloys [1, 2], *i.e.*, periodical stacking of closed-packed planes, which correspond to (0001) in hcp and {111} in fcc [3, 4], their order structures due to stacking faults (defects) or very small amounts of additive elements [5], strengthening due to deformation kinks [6]. However, to the best of our knowledge, the formation mechanism of LPSO phases has not been clearly elucidated.

Our interests lie in studying thermal stability, elasticity and acoustic attenuation of $Mg_{23}Al_3Y_4$ alloy, by determining twelve kinds of parameters containing dilational and shear attenuation coefficients. $Mg_{23}Al_3Y_4$ alloy is characterized by synchronized LPSO structure with $L1_2$ typed Al_6Y_8 clusters consisting of four close packed atomic layers forming local fcc stacking [7]. Ultrasonics is the only method available for measurement of high-frequency elastic moduli and loss that arise from atomic motions underlying relaxation processes [8]. As far as we know, however, no research work has been carried out previously on measurement of these elastic parameters for the ordered alloy, using both longitudinal and transverse wave velocities, V_l and V_s, respectively.

2. Experiment A Mg–Al–Y alloy ingot with nominal atomic composition of $Mg_{23}Al_3Y_4$ was produced by inducting melting a mixture of Mg (99.9 mass %), Al (99.99 mass %) and Y (99.9 mass %) metals in an argon atmosphere. The alloy ingot was casted as a fully cast alloy, and then heated at 823 K for 345.6 ks. In contrast to irregular arrangement of $L1_2$ clusters in Mg-Zn-Y and Mg-Al-Gd alloys [1-3], $Mg_{23}Al_3Y_4$ alloy is characterized by formation of ordered $L1_2$ structure without heat-hardening after casting. The specimen size is 23 mm in length, 5 mm in width and 2 mm in thick. The density is measured by the Archimedean method using distilled water at room temperature.

Twelve elastic and viscosity parameters (Young E, shear G and bulk moduli K, Lamè parameter λ, Poisson's ratio v, G/K, Debye temperature Θ_D, dilational α_l and shear α_s attenuation coefficients, dilational η_l, shear η_s and volumetric η_v dynamic viscosities) were measured along thick (c-axis) direction with an ultrasonic measuring system (TP-1001; Toshiba Tungaloy) at room temperature, using longitudinal and shear waves with a frequency of 5 MHz [9]. For calculation of Θ_D [10], based on ultrasonic method, we used 2 degrees of freedom and 2.864×10^{-27} m^3 as an average atomic volume. The transducers were contacted at both edges of the specimen under a pressure of 0.2 MPa, by water-free naphthenic

hydrocarbon couplant oil (Tungsonic Oil H). The detailed experimental procedures have been described previously [11].

3. Results

3.1. Thermal stability evaluation by *VEC* The thermal stability of metallic alloys can be evaluated by adjustment of the height of the Fermi level to the valence electron concentration (*VEC*) proposed by Bilz [12]. The *VEC* in the metallic alloys (II_A, III_B, IV_C, V_D, VI_E, VII_F,$VIII_G$) for metal/metal type of group II to VIII elements has been defined as follows:

$$VEC = II_A + III_B + IV_C + V_D + VI_E + VII_F + VIII_G, \quad (1)$$

where A, B, C, D, E, F and G are atomic fractions and $A + B + C + D + E + F + G = 1$. *VEC* provides useful tool for material evaluation and composition design such as stability of metallic compounds [13], solid solubility [14], and electronic bonding mode [15]. We first evaluate the stability of $Mg_{23}Al_3Y_4$ alloy in terms of *VEC*. The relation between *VEC* (2.54) and order-disordered transition temperature (*Tc*) of the $Mg_{23}Al_3Y_4$ alloy is shown at Fig. 1, along with the data for 55 kinds of amorphous alloys for metal/metal type. The stable region for formation of amorphous alloys is $2.6 < VEC < 5.3$. The amorphous alloys, which are formed by multiple orbital electron hybridization such as *spd* or *spf* [16], are characterized by a nonideal elastic behavior, which the volume-preserving (uniaxial shear) deformation dominates. Because we cannot detect distinct *Tc* for differential thermal analysis, we used *Tc* of 436.5 K from 0.5 *Tm* [17], where *Tm* is a melting temperature (873 K) of $Mg_{23}Al_3Y_4$ alloy. The $Mg_{23}Al_3Y_4$ alloy locates to a point (2.54, 436.5 K) near a critical amorphous alloy of $Ca_{65}Mg_{15}Zn_{20}$ with the lowest *VEC* (2.32) and *Tg* (379 K). Thus there is a possibility that $Mg_{23}Al_3Y_4$ alloy is a metastable like metallic alloy. Since *VEC* of Al_6Y_8 cluster is 3, formation of LPSO would be derived from *spf* multiple orbital electron hybridization.

3.2. Elasticity evaluation by *G/K* The secondary nonharmonity potential energy between pairs of atoms dominates directly real elastic moduli [10], and hence the elastic moduli are important parameters for structural or electronic evaluation of solids containing atomic contribution. Especially, elastic parameters (E, G, K, λ) provide a sensitive probe for real elastic evaluations. Four kinds of the elastic moduli were calculated by longitudinal and transverse wave velocities for $Mg_2)_3Al_3Y_4$ alloy and a represenrative Mg-based alloy, $Mg_{77.9}Li_{22.1}$ (Mg-7.5 mass% Li, mix phases of α and β), which provides exceptional workability due to bcc-β phase, high rigidity, high specufic strength and superlight weight. These results are presented in Table 1, along with density, longitudinal and transverse wave velocities. The $Mg_{23}Al_3Y_4$ alloy shows the almost same uniaxial volume-preserving deformation as $Mg_{77.9}Li_{22.1}$ one, but the former resists three-dimensional nonvolume-preserving deformation with mixed mode-II-mode-III in comparison with the latter. This would be characterized by LPSO structures with structural rigidity due to deformation kinks [3, 6].

Since the directional property of Poisson's ratio is designated by the quotient of lateral to longitudinal strain $e_{ij} = - S_{ij} / S_{ij}$ (i, j = 1, 2, 3) (where S_{ij} stands for the elastic compliance constants) for all possible orientations of the coordinate system, we evaluate Poisson's ratio from three-dimensional volume-nonpreserving elastic deformability of view. The changes in Poisson's ratio are of great interest as these directly affect the mechanical properties such as ductility/toughness [18].

On the other hand, the ratio G/K can be conveniently taken as a measure of elasticity [19], because the elasticity of solids cannot be evaluated by the elastic moduli themselves alone. The ratios of 21 kinds of metals and alloys, 16 kinds of ceramics and 29 kinds of amorphous alloys, solders and polymers containing rubbers at room temperature are shown in Fig. 2, as a function of Poisson's ratio, along with that of the $Mg_{23}Al_3Y_4$ alloy (insert). The ratio G/K of all materials correlates well to Poisson's ratio. When the ratio of the $Mg_{23}Al_3Y_4$ alloy at room

temperature is compared with those of other representative materials; for examples, carbon steel 0.619, Al 0.326, Cu 0.307, solder ($SnPb_{37}$) 0.363, TiAl 0.465, alumina 0.237, β‘-sialon 0.510, quarz 0.859, PMMA 0.414, PI 0.338, urethane rubber 0.348, the value (0.404) for the $Mg_{23}Al_3Y_4$ alloy is close to group region of amorphous alloys and polymers with high elasticity in volume-nonpreserving distortion, suggesting enhancement of toughness derived from formation of LPSO structures.

If a coupling of the phonons with a thermally activated relaxation process occurs [20], it will induce a change in Debye temperature. Next we calculated the elastic Debye temperature of two Mg-based alloys. Θ_D is calculated as 72.5 K for $Mg_{23}Al_3Y_4$ and 90.9 K for $Mg_{77.9}Li_{22.1}$. Θ_D of the former is smaller than that of the latter. Because ultrasonic wave velocities are dominated by soft region in complex material such as $Mg_{23}Al_3Y_4$ used in this study, decrease in Debye temperature, *i.e.* decrease in the maximum frequency allowed, indicates increase in effective atomic distance among Mg atoms due to periodical stacking of closed-packed planes.

3.3 Damping evaluation by acoustic attenuation Lastly, we investigate ultrasonic dispersion and viscoelasticity for Poisson's ratio in terms of complex elasticity. The damping properties for longitudinal and transverse waves are measured as a function of Poisson's ratio. Table 2 shows the attenuation coefficients for both receiving waves, along with those of $Mg_{77.9}Li_{22.1}$. Both coefficients of Mg-based alloys show higher danping properties compared with other metals (0.1~0.4) and amorphous alloys (0.07~1.6). This can be explained by twin boundaries and their reciplocating movements at high vibration strain amplitude [21].

The eventual thermodynamic behavior of Mg-based alloys closed to macromolecules must involve a Newtonian viscous component to the elastic response; such a situation is denoted as viscoelasticity, associated with complex waves. To investigate the viscoelastic

effect, we calculate dynamic viscosity η of the Mg-based alloys. Equation (2) can be synonymously expressed by a complex elasticity M^* [22],

$$M^* = M_1 + i\omega\eta, \quad (2)$$

where M_1 ($= \rho V^2$) is a dynamic elasticity. Next, we can use the following formulae for η_λ, η_σ and η_v,

$$\eta_\varpi = \eta_K + 4/3\,\eta_\sigma, \quad (3)$$

$$\eta_K = K/\omega, \quad (4)$$

$$\eta_\lambda = E/\omega, \quad (5)$$

$$\eta_\sigma = \Gamma/\omega, \quad (6)$$

where $\omega = 2\pi f$. These results are also presented at Table 2. The dilational, shear and volumetric dynamic viscosities are 1/5, 1/7 and 1 of amorphous alloys [11], respectively. These results indicate that viscoelasticity of the Mg-based alloys is predominated by three-dimensional volumetric motion, rather than one-dimensional one, showing high rigidity caused from formation of LPSO structures. Furthermore, the $Mg_{23}Al_3Y_4$ alloy of interests is known to an alloy with fairly stacking faults (vacancies [7]) among four Al-Y cluster layers, as well as amorphous polymers with large viscoelastic response have greater free volume [23].

4. Discussion In previous paper [24], we investigated the effect of excess electrons accommodated in hcp Mg and in the model Mg clusters using density functional theory (DFT)-based calculation in glass-forming abilities and thermal stabilities of Mg-based amorphous alloys. The c/a ratio in hcp Mg increases proportionally to the concentration of excess electrons and the cell volume expands. The pseudogap by *s*-*p* mixing at Fermi level is weakened in the expanded cell with a distorted c/a ratio and a new spiky structure mainly contributed by *p* bands appears. The expanded volume and the distorted c/a ratio by the charge transfer from additive elements such as Cu and Y suppress the crystallization of

supercooled liquid. On the other hand, the increase in the conduction electron concentration of Mg in amorphous alloy stabilizes the cluster structures. In brief, the conduction electron concentration in Mg-based amorphous alloys plays a definitive role for increase in c/a ratio and cell expansion, and stabilization of cluster structures.

By analogy, hence we infer that the formation of LPSO structures in Mg-based alloys is promoted by cell expansion accompanying increase in c/a ratio by appearance of excess electrons, resulting in stabilization of cluster structures in four close packed atomic layers. *VEC* values of the nine kinds of Mg-based alloys are presented at Table 3. These values are 2.45~2.54, while *VEC* values of Mg-based amorphous alloys are 2.63~3.29. This means that all Mg-based alloys with LPSO structures are composite alloys consisting main α-Mg crystalline phase and very small amount of an amorphous phase, $i.e.$, a metallic cluster. Thus the increase in the valence by addition of Al and Y elements into magnesium stabilizes the cluster structures and affirms positively the application of *VEC* for the electronic rule associated with the stability of Mg-based alloys [15]. The excess electrons are induced by addition of elements with large valence electrons and supercooling from liquid state. The transition and rare-earth metals are candidates for additive elements with large valence electrons [15, 16]. The resonance bondings of the former and the latter are caused by *spd* and *spf* hybridization, respectively [15, 16, 24]. Kawamura *et al*. [25] have succeeded development of higher strength Mg-based alloy, using supercooled powder metallurgy method [26].

Although the order of $K > \lambda > E > G$ in four elastic moduli is monopolistically characterized by amorphous alloys, the order of $Mg_{23}Al_3Y_4$ alloy in Table 1 is $E > K > \lambda > G$ as well as carbon steels, cast irons, Ni and Ti-based alloys in Table 4. This means that the formers show characteristic one-dimensional elastic deformability, while the latter displays volumetric (three-dimensional volume- nonpreserving) deformation with mixed mode-II-

mode-III. The formation of LPSO phase along c-axis in α-Mg phase effectively contributes to enhancement of strength for volumetric deformation [2, 3]. In this case, formation of $L1_2$ typed Al_6Y_8 clusters in LPSO phase induces local fcc vacancies (stacking faults) around its cluster, leading to strengthening due to deformation kinks [6]. Thus an addition of small amounts of transition and rare-earth elements, *i.e*. appearance of excess electrons plays an important role for formation of LPSO phases with clusters, resulting in increase of strength.

5. Conclusions

Characteristic elastic and viscoelastic behaviors of $Mg_{23}Al_3Y_4$ alloy with LPSO structures were examined in terms of *VEC* and complex elasticity. The set point (2.54, 436.5 K) of *VEC* and Tc for $Mg_{23}Al_3Y_4$ alloy shows a metastable like amorphous alloy. The addition of small amounts of Al and Y elements, *i.e*. appearance of excess electrons induces an increase in c/a ratio and cell expansion of hcp Mg lattice, and stabilization of cluster structures, leading to formation of LPSO phases with $L1_2$ typed Al_6Y_8 clusters derived from *spf* multiple orbital electron hybridization. The alloy with higher Poisson's ratio and the lower ratio *G*/*K* in metallic group suggest a metastable like metallic alloy in elasticity. From dilational, shear and volumetric dynamic viscosities, the viscoelasticity of the alloy with stacking faults (vacancies) is predominated by three-dimensional volumetric motion.

References

[1] E. Abe, Y. Kawamura, K. Hayashi and A. Inoue, Acta Mater. **50**, 3845-3857 (2002).

[2] E. Abe, A. Ono, T. Itoi, M. Yamasaki and Y. Kawamura, Philo. Mag. Lett., 91, 690-696 (2011).

[3] S. Yoshimoto, M. Yamasaki and Y. Kawamura, Mater. Trans. **47**, 959-965 (2006).

[4] M. Matsuura, K. Konno, Y. Yoshida, M. Nishijima and K. Hiraga, Mater. Trans., **47**, 1264-1267 (2006).

[5] C. Koening, N. Stefanou and J. M. Koch, Phys. Rev. B., **33**, 5307-5318 (1986).

[6] K. Hagihara, N. Yokotani and Y. Umakoshi, Intermet. **18**, 267-276 (2010).

[7] D. Egusa and E. Abe, Acta Mater., **60**, 166-178 (2012).

[8] M. Fukuhara, A. H. Matsui, and M. Takeshima, Chem. Phys. **258**, 97-106 (2000).

[9] M. Fukuhara, M. Yagi & A. Matsuo, Phys. Rev., **B65**, 224210 (2002).

[10] O. L. Anderson, J. Phys. Chem. Solids, **12**, 41-52 (1959).

[11] M. Fukuhara, W. Zhang and A. Inoue, Phys. Stat. Sol., A. **204**, 3116-3120 (2007).

[12] H. Bilz, Z. Phys. **153**, 338-358 (1958).

[13] M. Fukuhara, T. Mitsuda, Y. Katsumura, and A. Fukawa, J. Mater. Sci., **20**,710-717 (1985).

[14] M. Fukuhara and H. A. McKinstry, Phys. Stat. Sol. B, **157**, 357-377 (1990).

[15] M. Fukuhara, M. Takahashi, Y. Kawazoe and A. Inoue, Appl. Phys. Lett., **90**, 073114 (2007)

[16] M. Fukuhara, M. Takahashi, Y. Kawazoe and A. Inoue, J. Alloy Comp., **483**, 623-636 (2009).

[17] K. Sumino, Physical Properties of Metallic Compounds, (Japan Metallurgy Society, Sendai, 1971), p.75.

[18] J. J. Lewandowski, W. H. Wang, and A. L. Greer, Philos. Mag. Lett. **85**, 77-87 (2005).

[19] R. Kubo in *Elasticity in Rubber* (Japanese), p.78 (Shokabo, Tokyo, 1996).

[20] O. L. Anderson and H. E. Bömmel, J. Amer. Ceram. Soc., **38**, 125-131 (1955).

[21] Y. Cui, Y. Li, S. Sun, H. Bian, H. Huang, Z. Wang, Y. Koizumi and A. Chiba, Scripta Mater., **101**, 8-11 (2015).

[22] A, W. Nolle and P. W. Sieck, J. Appl. Phys., **23**, 888-894 (1952).

[23] M.H. Cohen, G.S. Grest, Phys. Rev. B **20**, 1077-1098 (1979).

[24] M. Takahashi, M. Fukuhara, A. Inoue and Y. Kawazoe, J. Phys. D: Appl. Phys. **41**, 155424 (2008).

[25] Y. Kawamura and S. Yoshimoto, Magnesium Technology, ed. by H. I. Kaplan, TMS, 499-502 (2005).

[26] H. Okouch, Y. Seki, T. Sekigawa, H. Hira and K. Kawamura. Mat. Si. Forum, **638-642**, 1476-1481 (2020).

Table 1 Density, wave velocities *Vl*, *Vs* and four elastic moduli for $Mg_{23}Al_3Y_4$ and $Mg_{92.5}Li_{7.5}$ alloys.

Mg-based alloys	Density (Mg/m^3)	V_l (m/s)	Vs (m/s)	E (GPa)	G (GPa)	K (GPa)	λ (GPa)
$Mg_{23}Al_3Y_4$	2.56	4,781	2,450	40.61	15.36	38.02	27.78
$Mg_{77.9}Li_{22.1}$	1.487	5,382	3,102	35.8	14.31	23.99	14.46

Table 2 Dilational α_l, and shear α_s attenuation coefficients, and dynamic dilational, shear and volumetric dynamic viscoelasticities, η_l, η_s and η_v, respectively for $Mg_{23}Al_3Y_4$ and $Mg_{77.9}Li_{22.1}$ alloys.

Mg-based alloys	α_l (Nep/cm)	α_s (Nep/cm)	η_l (Pa· s)	η_s (Pa· s)	η_v (Pa· s)
$Mg_{23}Al_3Y_4$	6.1	1.25	1,291	488	1,860
$Mg_{77.9}Li_{22.1}$	8.93	6.45	1,138	455	1,369

Table 3 *VEC* values of Mg-based alloys with 9 kinds of LPSO structures.

material	$Mg_{23}Al_3Y_4$	$Mg_{97}ZnY_2$	$Mg_{96}Zn_2Y_2$	$Mg_{96}Co_2Y_2$	$Mg_{96}Ni_2Y_2$	$Mg_{96}Cu_2Y_2$	$Mg_{96.7}Zn_{0.85}Y_2Al_{0.45}$	$Mg_{96.65}Zn_1Y_2Al_{0.45}$	$Mg_{93.5}Ni_3Y_{3.5}$
VEC	2.54	2.448	2.484	2.486	2.488	2.48	2.463	2.445	2.535

Table 4 Density, wave velocities and four elastic moduli for 21 kinds of metals and alloys, 16 kinds of ceramics and 29 kinds of amorphous alloys, solders, polymers and rubbers at room temperature.

materials	density (g/cm3)	*Vl* (m/s)	*Vs* (m/s)	*E* (GPa)	*G* (GPa)	*K* (GPa)	λ (GPa)	ν	*G*/*K*
mild steel (S10C)	7.889	5773.1	3361.5	221.704	89.1432	144.07	84.644	0.2435	0.619
mild steel (S45C)	7.888	5944.4	3225.7	211.972	82.0757	169.3	114.58	0.2913	0.485
stainless steel (SUS304)	7.899	5831.8	3172.5	205.088	79.5015	162.64	109.64	0.2898	0.489
stainless steel (SUS316L)	7.946	5939.4	2751.4	164.023	60.1528	200.1	160	0.3634	0.301
ferrite stainless steel (SUS430)	7.7	4596.7	1723.1	64.8479	22.8619	132.22	116.97	0.4183	0.173
stainless steel (SUS331)	7.75	6996.6	3327.7	232.372	85.8203	264.95	207.74	0.3538	0.324
stainless steel (SUS332)	7.75	6896	3350.7	234.141	87.0107	252.54	194.53	0.3455	0.345
stainless steel (SUS630)	7.764	6102.4	3233.3	211.82	81.1666	180.9	126.79	0.3048	0.449
ductile cast iron (FCD100)	7.052	5514.7	3051.4	168.01	65.6615	126.92	83.142	0.2794	0.517
alloy tool steel (SKD11)	7.977	5950.2	3251.9	217.141	84.3556	169.95	113.71	0.2871	0.496
Ni	8.897	8866.1	2773.5	197.892	68.4384	608.12	562.5	0.4458	0.113

Al	2.717	6443.8	3071.3	69.3536	25.6291	78.645	61.559	0.353	0.326
Al cast alloy	2.677	6522	3218	74.38	27.72	78.33	59.85	0.342	0.354
oxygen-free copper	8.936	4812.9	2309.9	128.768	47.6793	143.42	111.64	0.3504	0.332
MgLi7.5	1.487	5382	3102	35.69	14.31	23.51	13.97	0.2513	0.609
Mg cast alloy	1.808	5810	3066	44.42	17	38.28	26.95	0.307	0.444
Ti-6Al-4V	3.896	6444.2	3140.1	103.285	38.4154	110.57	84.961	0.3443	0.347
Ti6242	4.546	6068	3110	116.243	43.9694	108.76	79.448	0.3219	0.404
Ti	4.5	6255	3237	124.209	47.1518	113.19	81.759	0.3171	0.417
INCONEL 718	8.31	5862.4	3108	209.433	80.2718	178.57	125.05	0.3045	0.45
Hasteloy C-276	8.793	4977.1	2724.6	167.891	65.2744	130.78	87.267	0.286	0.499
NCF600	8.354	5934.7	2702.3	167.057	61.0045	212.89	172.22	0.3692	0.287
Cobal	8.1396	5105	2505	137.03	51.0762	144.02	109.97	0.3414	0.355
sterite	8.409	5758	3154	215.094	83.6503	167.26	111.5	0.2857	0.5
Ti-Nb	5.7427	5522	2540	101.206	37.0496	125.71	101.01	0.3658	0.295
solder (Sn-37Pb)	8.407	2882.6	1336.5	40.9385	15.0169	49.835	39.823	0.3631	0.301
solder (Zn-3Al)	6.783	3829	2397	91.8019	38.9725	47.484	21.502	0.1778	0.821
solder (Sn-6Zn)	7.2556	2976	1434	40.2485	14.9201	44.366	34.42	0.3488	0.336
solder (Sn-9Zn)	7.2772	2998	1455	41.4713	15.406	44.866	34.595	0.3459	0.343
solder (Sn-12Zn)	7.2658	3198	1468	42.7937	15.658	53.432	42.993	0.3665	0.293
solder (Sn-40Zn)	7.2361	3407	1628	51.8606	19.1784	58.423	45.637	0.3521	0.328
splder (Sn-1Bi)	7.2717	3455	1771	60.2935	22.8073	56.393	41.188	0.3218	0.404
solder (Sn-3Bi)	7.3393	3416	1743	59.043	22.2972	55.913	41.048	0.324	0.399
W	13.3	4163.3	2353.1	186.361	73.6432	132.34	83.243	0.2653	0.556
TiAl	4.006	7332.6	3930.2	160.693	61.8786	132.89	91.634	0.2985	0.466
TiNi	6.459	4755	1732	55.1636	19.3759	120.2	107.29	0.4235	0.161
PdDx	7.1559	4522	1766	62.9361	22.3175	116.57	101.69	0.41	0.191
Mn73Cu20Ni5Fe2 (M2052)	7.317	3878	2508	104.983	46.0244	48.674	17.991	0.1405	0.946
Ti6242-10TiB2	4.56	6416	3358	134.859	51.4193	119.15	84.874	0.3114	0.432
Ti6242-20TiB2	4.563	6736	3656	157.502	60.9906	125.72	85.059	0.2912	0.485
Pd40Cu30Ni10P20	9.285	4860	1901	94.6013	33.5541	174.57	152.2	0.4097	0.192
Cu45Zr45Ag10	7.913	4652	2095	95.24	34.7304	124.94	101.79	0.3728	0.278
Cu46Zr46Al4Ag4	7.3613	7657.1	2071.9	92.307	31.6012	389.46	368.4	0.4605	0.081
Zr65Ni10Cu5Al17.5Pd12.5	7.127	4491.1	1984.7	77.4059	28.0729	106.32	87.603	0.3787	0.264
Cu60Zr30Ti10	7.4308	6476.3	2594.6	140.504	50.0226	244.97	211.62	0.4044	0.204
Ti41.5Cu42.5Ni7.5Hf5Zr2.5Si1	6.6902	6440.1	2512.4	126.9	42.23	221.2	193.04	0.4102	0.191
ZrO2-3molY2O3	6.05	7045	3652.6	212.474	80.716	192.65	138.84	0.3162	0.419
Si3N4-4AlN-8Y2O3	3.27	10600	5927.6	292.411	114.896	214.22	137.62	0.2725	0.536
Si3N4	3.204	11436	6299.6	326.058	127.151	249.48	164.71	0.2822	0.51
α-SiC	2.98	11217	7132	351.874	151.579	172.84	71.789	0.1607	0.877
α-Al2O3	3.954	10840	6367.8	396.507	160.33	250.83	143.94	0.2365	0.639
Al2O3-30Ti(C,N)	4.3	10435	6164.9	402.655	163.426	250.33	141.38	0.2319	0.653
Al2O3-20Zr2O3	5	8616.8	4792.4	293.077	114.835	218.13	141.58	0.2761	0.526
Al2O3-30SiCw	2.79	7457	3881.4	110.477	42.0321	99.1	71.079	0.3142	0.424
MgO	3.374	9460	5822	273.367	114.364	149.46	73.217	0.1952	0.765
graphite	2	3059.9	1873.3	16.848	7.01851	9.368	4.689	0.2003	0.749
h-BN	1.8	5412.4	2076.6	21.9464	7.76208	42.38	37.205	0.4137	0.183
c-BN	4.04	13128	8533.3	667.323	294.182	304.05	107.93	0.1342	0.968
WC	15.999	17418	9644.9	3806.75	1488.29	2869.5	1877.4	0.2789	0.519
GdBa2Cu3O8-x	4.768	3189.4	1825.7	39.9322	15.8926	27.311	16.716	0.2563	0.582
BaTiO3	5.9185	8261	4735	333.159	132.694	226.98	138.51	0.2554	0.585

CaTiO3	7.56	5914	3901	256.528	115.047	111.02	34.321	0.1149	1.036
fuzed quartz	2.22	5964.4	3773.7	73.7398	31.6146	36.822	15.745	0.1662	0.859
mica ceramic	3.01	6355.2	3574.3	97.5701	38.4535	70.298	44.662	0.2687	0.547
alumina brick	3.29	6866.5	3750.9	119.177	46.2878	93.403	62.544	0.2873	0.496
magnesia brick	2.528	4281.1	1986.8	27.1977	9.97896	33.027	26.375	0.3628	0.302
Ti(C,N)-Mo2C-Ni	6.957	8377	5054.2	431.427	177.716	251.25	132.77	0.2138	0.707
polymethyl methacrylate (PMMA)	1.187	2692	1390	6.04648	2.2934	5.5442	4.0152	0.3182	0.414
polycarbonate (PC)	1.185	2330	1198	4.49097	1.70072	4.1656	3.0318	0.3203	0.408
polyethylene (PE)	0.944	2248.4	878.5	2.05437	0.72854	3.8008	3.3151	0.4099	0.192
polyethylene terephthalate (PET)	1.59	2274.9	820.8	3.05329	1.0712	6.8002	6.0861	0.4252	0.158
polyether imide (PEI)	1.34	2374	1035	3.96946	1.43544	5.6382	4.6812	0.3827	0.255
polysulfone (PSF)	1.24	2220	910	2.87315	1.02684	4.7421	4.0575	0.399	0.217
polyether sulphonw (PES)	1.37	2260	930	3.31319	1.18491	5.4175	4.6276	0.3981	0.219
polyphenylene sulfide (PPS)	1.3	2560	1020	3.80232	1.35252	6.7163	5.8146	0.4056	0.201
polyimide (PI)	1.488	3046	1470	8.67001	3.21542	9.5186	7.375	0.3482	0.338
epoxy resin	1.202	3097.9	1447	6.84796	2.51676	8.1799	6.5021	0.3605	0.308
polyamide imide	6.459	5047.2	2042.1	75.533	26.9351	128.62	110.67	0.4021	0.209
polyvinyl chloride (PVC)	1.377	3048	1435	7.69917	2.83555	9.012	7.1216	0.3576	0.315
urethane rubber	1.075	1731.5	843.8	2.05781	0.7654	2.2024	1.6922	0.3443	0.348
styrene-butadiene rubber (SBR)	1.1106	1730.9	701.9	1.53378	0.54715	2.5978	2.2331	0.4016	0.211
anthracene	1.256	3001.3	1554.8	7.99505	3.03626	7.2655	5.2413	0.3166	0.418
nitrile silicone rubber (NS520)	1.15	1912.5	236.5	0.19197	0.06432	4.1205	4.0777	0.4922	0.016

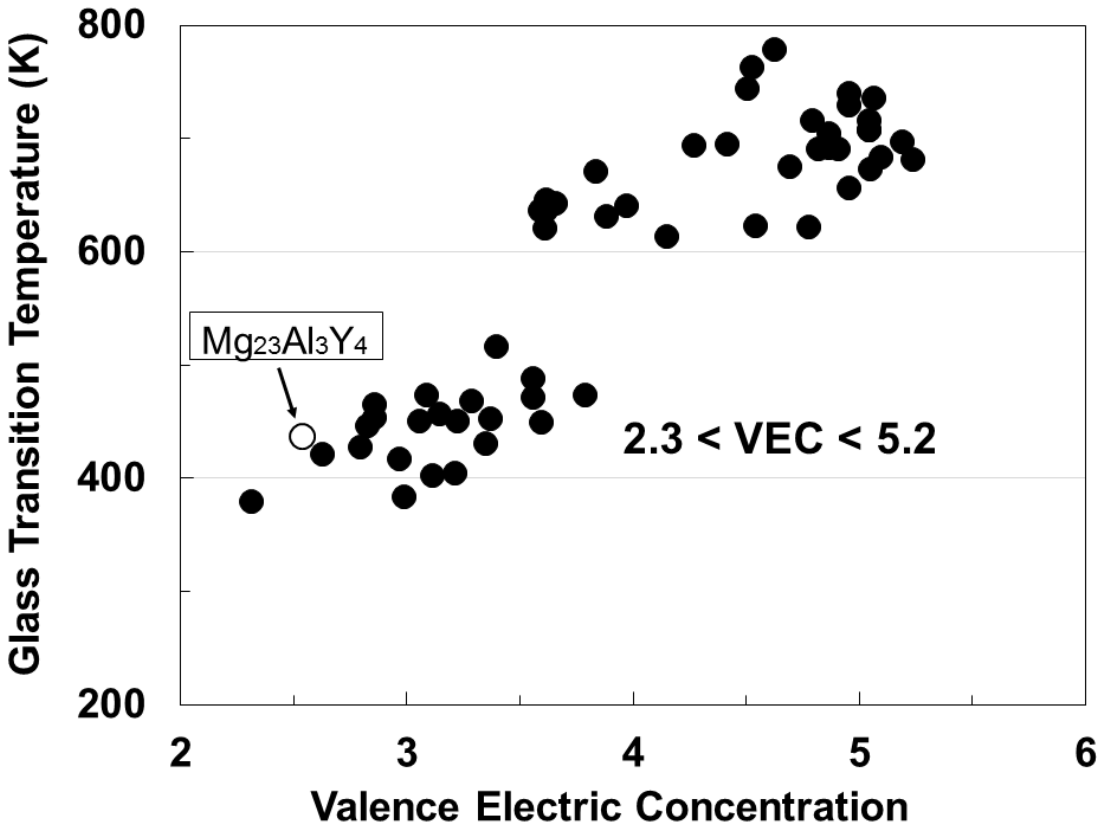

Fig.1 Relation between *VEC* (2.54) and estimated order-disordered transition temperature (*Tc*) of the $Mg_{23}Al_3Y_4$ alloy in comparison with relation between *Tg* and *VEC* for 55 kinds of amorphous alloys for metal/metal type.

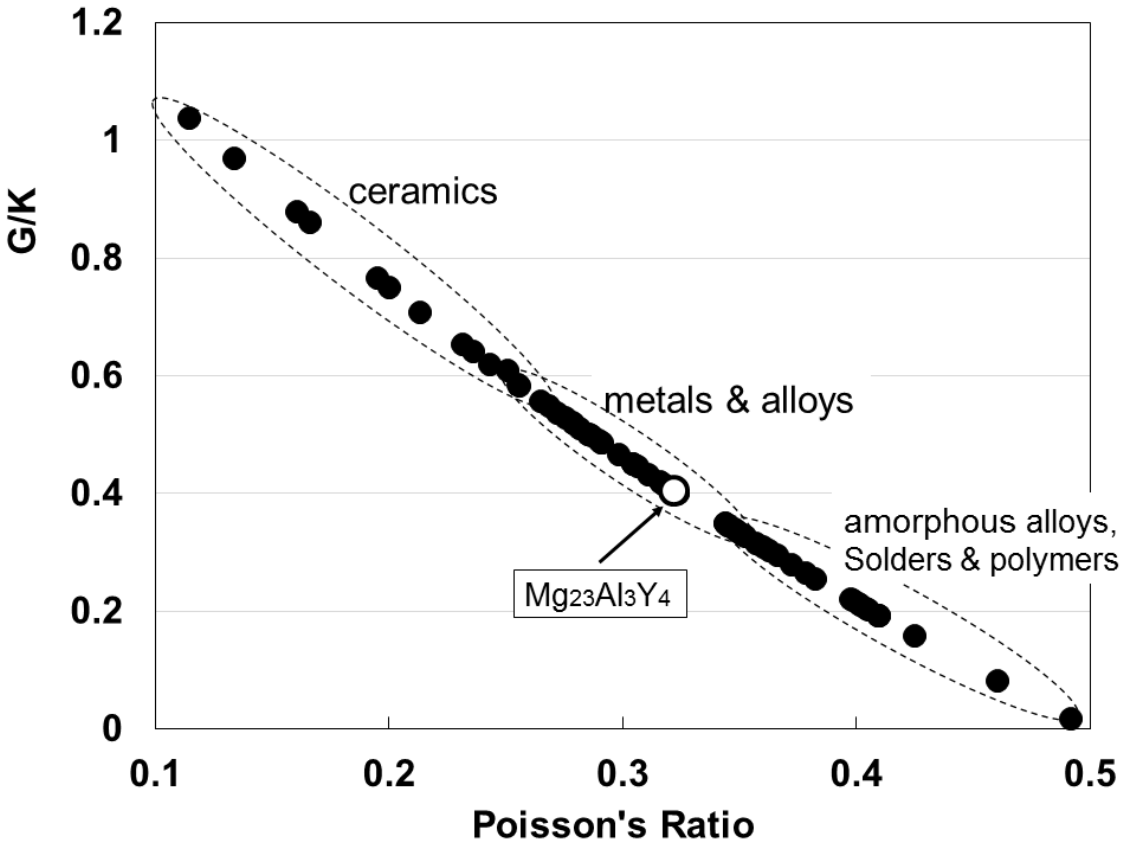

Fig. 2 The relation between *G/K* and Poisson's ratio of $Mg_{23}Al_3Y_4$ alloy in comparison with the relation between *G/K* and Poisson's ratios of 43 kinds of metals and alloys, 22 kinds of ceramics and 30 kinds of polymers and rubbers.